



## Investigating the effects of defects and the effect of geometric anisotropy in stainless steel pipes: phased array ultrasonic test, SH-wave

Esmaeil Mirmahdi\*, Ramin Khamedi, Davood Afshari, Mehdi Khosravi

University of Zanjan, Faculty of Engineering, Department of Mechanical Engineering, Zanjan, Iran



### ARTICLE INFO

#### Keywords:

Phased array ultrasonic testing  
Non-destructive testing  
Experimental results  
Finite element  
Geometric anisotropy

### ABSTRACT

Today, Phased Array Ultrasonic Testing (PAUT) is a suitable method for detecting defects in Non-destructive Testing (NDT). This simulation was done with a new method on a stainless steel pipe with a diameter of 500 mm and a length of 1,000 mm, and cracks were modeled on the external and internal surfaces and corrosion defects on the internal surface. Four probes with a characteristic of 2 MHz were used simultaneously, each probe having 64 elements. By increasing the number of probes and their elements, more accurate information about the defects is obtained, which makes it easier to detect the location and leads to a reduction of scattered signals and noise, which can detect even small size defects. Considering this important advantage, a new use of the method of increasing the number of probes in PAUT is reported in this study to detect defects, especially corrosion defects. The results of geometric anisotropy studies of group velocity and phase of horizontally polarized shear waves (SH-waves) for stainless steel pipe were presented. Due to the isotropic properties of the pipe material, the speed on the outer surface of the pipe in the direction of the cover is 40 m/s higher than the generatrix.

### 1. Introduction

Phased Array Ultrasonic Testing (PAUT) is one of the new methods that is used as a Non-destructive Testing (NDT) and uses the Ultrasonic Testing (UT) method (Wilkinson and Duke, 2014). The advantages of this test over other ultrasonic methods include the detection of defects in the shortest time and the ability of the sound beam to be guided, scanned, and focused electronically (Ahmed et al., 2021). The PAUT uses multi-element probes, each operating separately under computer control with a time delay (Brigante and Sumbatyan, 2013). The propagation path of the generated wave depends on the arrangement of time delays (Malinowski et al., 2009). Probes are ultrasonic transmitters and receivers that each of these elements is excited independently and with a certain time delay (Schabowicz and Suvorov, 2014). By proper timing of time delays to excite the elements, it can be produced and directed a beam bundle with a specific path inside the part (Tran et al., 2022). In addition to propagating the waves, the probe is also responsible for receiving the response caused by the echo of the waves, which is coordinated between sending and receiving it by the main processor. In addition to the ability to direct the generated beam in a certain direction, these types of probes can send waves at a specific point (Rosa and Yang, 2020). It allows the beam conduction feature in the step array test method the angles of the selected beams to be guided in such a way

that they collide vertically with some of the predicted defects in the test piece while moving and displaying them (Shevtsov et al., 2020).

In addition to the stated advantages due to the complexity of PAUT probes, there are also cases in simulation, design, and use, such as the proper adjustment of time delays to deliver the beam and focus it at the desired point, a large number of received data (Liu et al., 2022). The PAUT applications also include inspection of pipes, an inspection of composite materials and forged parts, welding inspections, an inspection of hydrogen cracking, and an inspection of complex components such as reactors and turbines. The PAUT is also used to inspect thick-walled pipes in a nuclear power plant (Azari and Kok, 2022). It is noteworthy that by analyzing the acoustic pressure distribution of ultrasonic waves performed by a PAUT probe, the transmitted wavelength and the angle of the beam orientation affect the efficiency of this type of probe (Dolmatov et al., 2019). Also, due to the complexity of ultrasonic wave propagation in heterogeneous and anisotropic environments, finite element simulation environments greatly contribute to the inspection process and the correct understanding of how the waves propagate and the results obtained in them (Fendzi et al., 2014; Qin et al., 2019). There are many defects in the welded part of oil and gas pipes, and their measurement by the PAUT method will be very useful. Also, the presence of impurities inside the pipes causes the pipes to become damaged in the long run (Liu et al., 2022; Groysman, 2019; Chauveau, 2018). In

\* Corresponding Author.

E-mail address: esmaeilmirmehdi69@yahoo.com (E. Mirmahdi).

stainless steel pipes, along with texture anisotropy, there is also geometric anisotropy due to the influence of wall curvature. In this case, the geometric anisotropy depends significantly on the tube geometry (diameter, wall thickness), as well as on the frequency of oscillation and the type of guided wave. The focusing algorithms with the equations presented in the paper are usually implemented assuming that the speed of the guided wave is constant in all directions (Hakoda et al., 2018; Murav'eva and Murav'ev, 2016; Satyanarayan et al., 2007). Propagation of shear waves (SH-waves) in the pipe by excitation from concentrated sources, which is focused, occurs in a wide range of different angles of the pipe, and the path of travel is not only limited to the directions along and across the pipe axis, but also along spiral lines in flat isotropic conditions at low frequencies, the zero mode SH-wave has a constant velocity in any direction. At higher frequencies, depending on the sheet thickness, higher order SH-wave modes appear with velocity dispersion (Frederick et al., 2010). The PAUT method is effective for inspecting Butt Fusion joints (BF) in HDPE pipes. Factors that affect this type of pipe are the joint point, wall thickness, and temperature (Shi et al., 2020; Mirmahdi, 2021).

In this research, by designing and presenting a new solution, a simulation of the PAUT method is presented for measuring defects in stainless steel pipes which has been done experimentally and simulated, the propagation behavior of ultrasonic waves is analyzed by four probes simultaneously, which makes external and internal crack defects easier to detect. In this method, Gaussian pulse is used for the simulated wave model and the occurrence of pipe defects with a new simulation solution and its size is shown by PAUT probes. Geometrical anisotropy was also investigated by SH-wave in stainless steel pipes, and the results of the velocity on the outer surface of the pipe.

## 2. Experimental test (PAUT)

The experimental test is performed by a linear converter and three pipes with three artificial defects created. The pipe on which the test operation is performed is made of stainless steel with a length of 100 cm, a thickness of 7 mm, and a diameter of 50 cm. Internal and external cracks are caused by the milling machine and corrosion by a drill in the form of a hole with a thickness of 5 mm. The depth of the internal and external cracking defect and the depth of the corrosion defect were considered to be 3 mm. Each crack has a specific depth, which is considered according to the defects observed in the industry, and the depth makes it easier to detect the location of the defect, and the greater the depth, the easier it is to detect the defect. A 30-degree wedge made of Plexiglas is used to orient the PAUT at a fixed angle. This angle was obtained by determining the speed of the wave in the shoe. The ultrasonic pulse was recorded by a 64-element linear array, the parameters of which are shown in Table 1. Four probes were considered for the pilot test and the best result can be obtained by considering the best location for the probe on the pipe for the defect. This proposed method was successful. We place four probes at an equal distance on the pipe, and the farthest probe from the pipe is also able to detect acid defects, but in smaller dimensions in S-scan. All signals were sampled at frequencies of 2 MHz. In the experimental test, sometimes it was not possible to detect the defect in the pipe, or for some reason, the waves passed through the defect to receive the defect signal. This defect will be solved by the method of placing four probes on the pipe simultaneously. This defect is solved by placing four probes on the pipe at the same time. For example, it is possible to detect corrosion defects even with a small size, which will cause

damage to the pipe in the long run, and timely detection can greatly help the life of the pipe. This issue in the real program can also benefit from this mentioned method, or as in the past, a lot of time will be spent to find the defect. Fig. 1 shows a schematic of the defects on the pipe and Fig. 2 shows an experimental test and the placement of four probes on the pipe.

In the experimental results, Probe 1 reports the best results in terms of latency and echo arrival time to receive the defect signal. Also, Probe 4 does not give us a good signal of the defect due to its distance from the defect location. In very small size corrosion defects, wave passage was obtained in the experimental test, which is considered important and necessary by placing the probes in four different places and increasing the number of probes and their elements to detect and measure the defect. The results indicate that to identify the defect, the test should be performed several times to determine its exact amount, and the location of the probe is very important when performing the test. The method performed in this article is recommended, it is an easier method to find defects and its modeling can also be done for non-destructive tests, which is the first time. Fig. 3 shows the crack defect measurement by four probes. Since the internal and external cracks are very similar in shape and size, the results are almost identical. Fig. 5 shows the corrosion defect measurement by four probes. At this stage, we do not know in which part of the pipe the corrosion defect is, and it is interesting the issue of using four probes with the obtained results. Probe 1 to 3 do not show the exact results of corrosion defects, while Probe 4 shows the diagnosis of corrosion defects and their size. Fig. 7 shows finding the defect by not knowing the position of the defect. This image indicates the best position of the probe and the need to use four probes in one tube, so that the results are completely accurate. Figs 4, 6, and 8 show the results of the A-scan in the defect during the PAUT method; it was performed to accurately measure the S-scan defect. Detailed measurements were repeated several times and they are given the resulting echoes of internal and external cracking defects and corrosion defects in Table 2. It is reported internal crack defect size for Fig. 3 in the experimental test by S-scan 37 mm. It is the accurate measurement of the side of the probe that has the best location to identify the defect. The size of the pipe corrosion defect is reported to be 21 mm. This is the exact size of the probe, it has the best place to detect the fault. In Fig. 7, which was analyzed for very fine corrosion defects and its size and location of the best probe out of four probes, probe number 4 was reported. The size of the corrosion defect is reported to be 10.5 mm. This size is also reported for return waves from defects in the A-scan. See the measurements of return echoes in the experimental test in Table 2. The numbers in Table 2 show the exact size of the defect, if the size of the defect is different, their size will definitely change. These accurate results were obtained from the best selected location of the probe on the tube. The

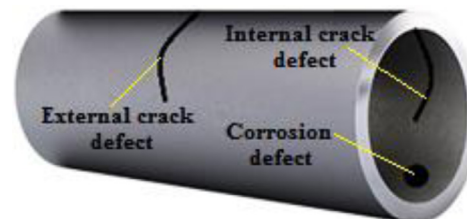


Fig. 1. Schematic of defects created on the pipe.

**Table 2**  
Measurement of return echoes from experimental test.

Return echoes from internal and external crack defects (mm)	Return echoes from corrosion defects (mm)	Return echoes from naturally occurring corrosion defects (mm)
37.0, 37.1, 37.3, 36.9	21.0, 21.1, 21.2, 20.9	10.5, 10.5, 10.6, 10.4

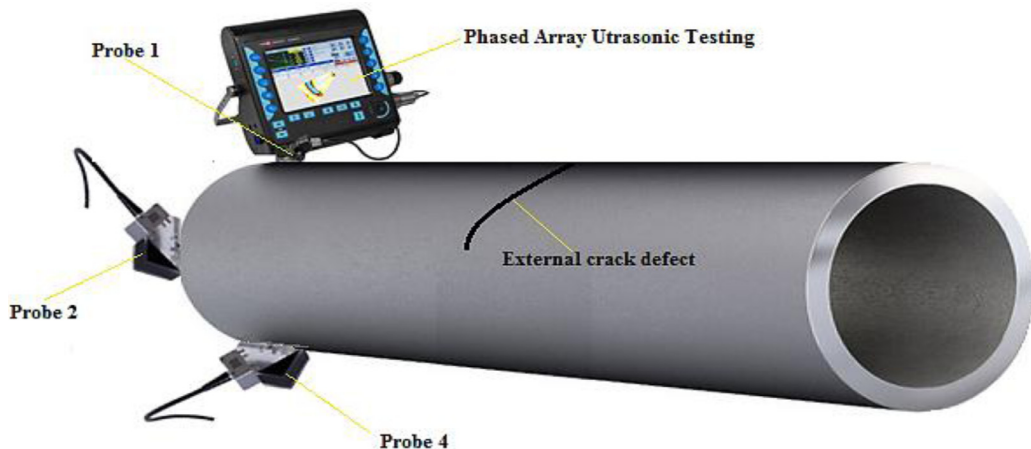


Fig. 2. PAUT test and placement of four probes on the pipe.

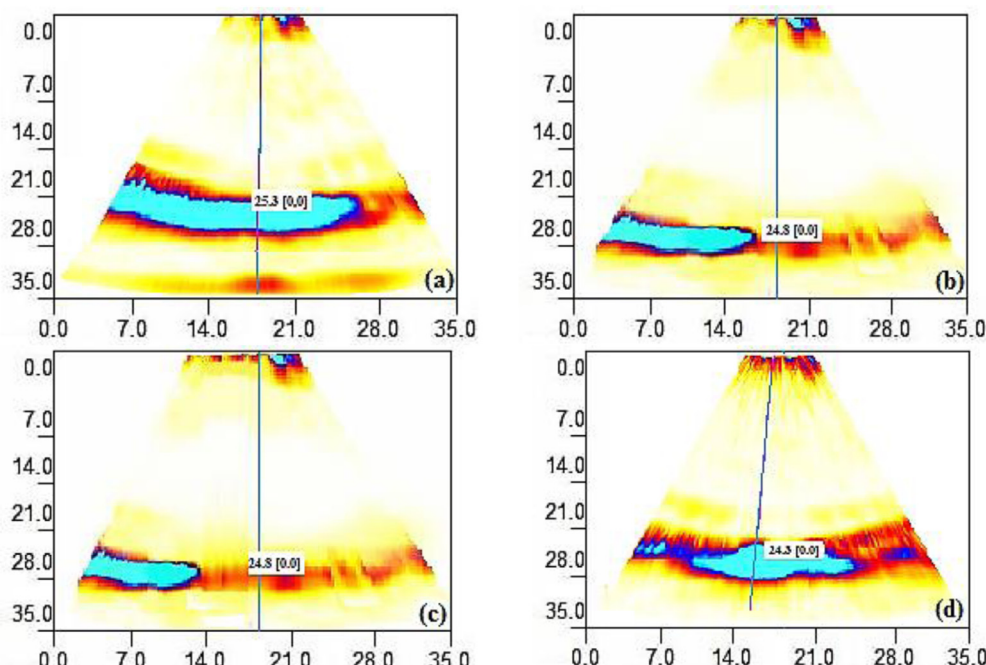


Fig. 3. PAUT test on external crack defect: (a) results of Probe 1; (b) results of Probe 2; (c) results of Probe 3; and (d) results of Probe 4.

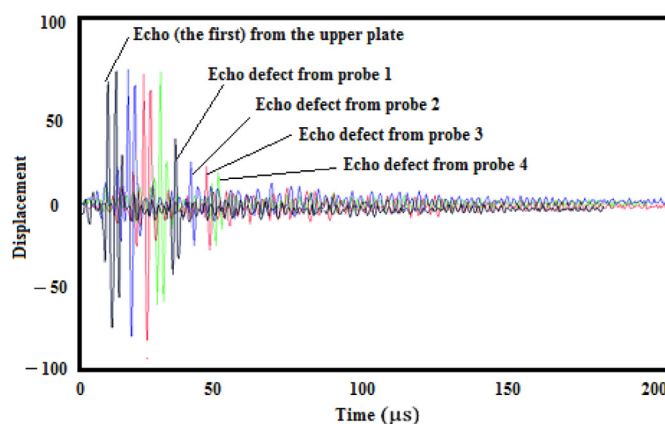
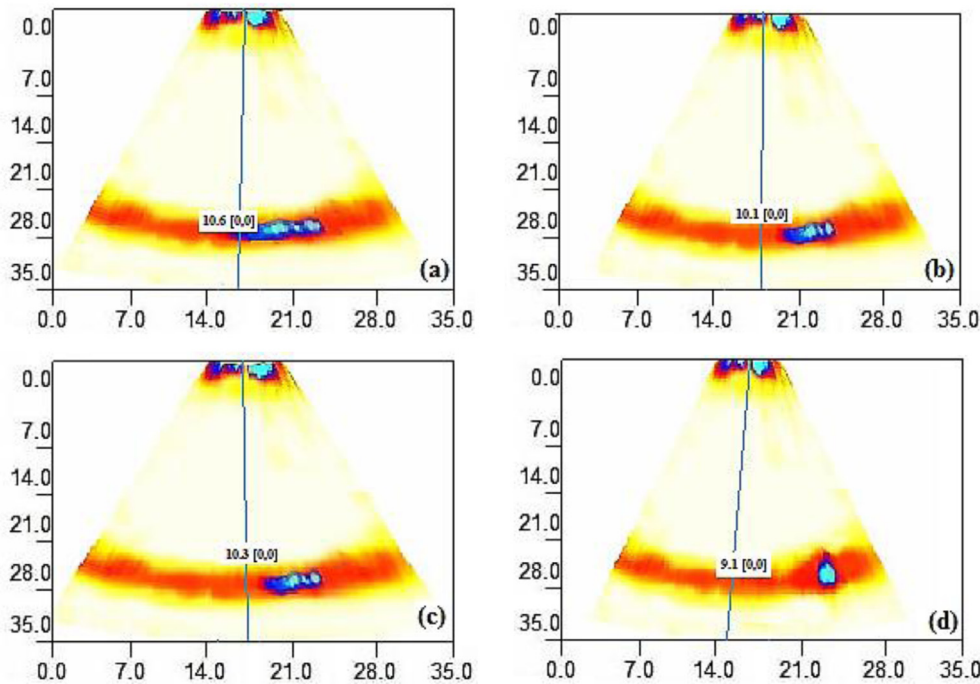
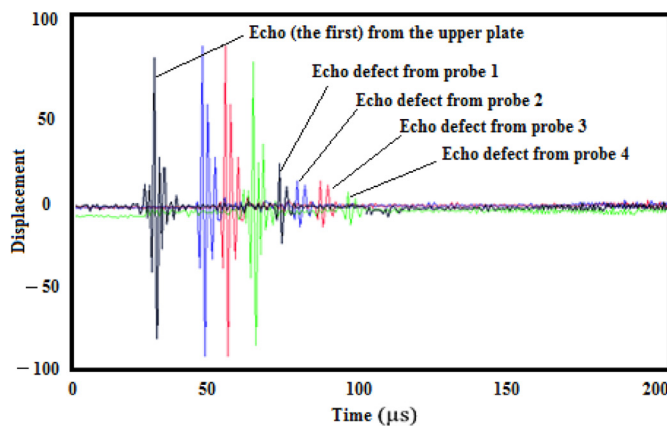


Fig. 4. Return echoes from internal and external crack defects.

color of all the defects in the PAUT display in the images obtained from the defect was assumed to be pale blue. The x-axis shows the length of the crack and the y-axis shows the width of the crack. It is the arc of the device itself that the blue color inside it determines the size of the defect. The crack is artificially created by the stone machine and has a very small size width that it was considered. The shapes that are seen the same are from Probes 2 and 3, which are almost at the same distance from the image to the defect, and their size is almost the same, but they are completely different, even the angle of their placement is different. It is considered the unit of the obtained shapes based on the angle of their placement for internal and external cracks between 23 and 25 degrees and for corrosion defects between 9 and 10 degrees; and these images are considered in the entire range and the results. Our completeness has been in the determined angles, and its other shapes were not considered. A-scan forms have a certain complexity, but to reduce this complexity and existing noises, the Wiener filter has been applied to all A-scans. The Wiener filter minimizes these noises and determines the size of the defect in the obtained signal processing and the exact size



**Fig. 5.** PAUT test on corrosion defect: (a) results of Probe 1; (b) results of Probe 2; (c) results of Probe 3; and (d) results of Probe 4.



**Fig. 6.** Return echoes from corrosion defects.

of the defect (Mirmahdi, 2020). The noises are reduced approximately and completely by the applied Wiener filter and wavelet transformation, which indicated the exact sizes and allows comparing the size of the defect with the simulation results.

For the concepts of shapes, it is necessary to explain briefly about display systems: In the A-scan system, the horizontal axis of the image plate is a symbol of thickness and the vertical axis indicates the intensity of reflection of the wave range. By interpreting the signals received from the wave response, the shape, size, type and position of the defects are evaluated.

In the B-scan system, the basis of the calculation of time changes is based on the distance traveled by the waves, and the view of the entire reflecting area of the waves will be seen on the screen in the form of a cross-section. One axis shows the linear movement of the probe and the other axis shows the time traveled by the waves.

The mechanism of C-scan electronic circuits also follows the pulse echo technique like the previous two systems, and their main difference is in a circuit known as the penetration depth determiner. With the help of this circuit, any depth of the thickness of the tested parts is arbitrarily

covered by the waves and the depth of the defect determined. In this way, after seeing the view of a defect in the image, the thickness of the piece is classified into several layers up to the border of the waves hitting the surface of the defect. In this case, the time taken by the waves to hit the layer containing the defect will indicate the depth of the defect.

### 3. Simulation

#### 3.1. Modeling pipes and pulses

If the displacement of particles in all three directions is axial, peripheral, and radial in simulating the propagation of waves in a pipe, we are required to use a three-dimensional model. Three-dimensional modeling is the most comprehensive model and the results will be accurate, but the computer computation time is high, especially when the modeling is at high frequency or large dimensions of the structure. To model, the Comsol software has been used in this paper. According to the presented shapes of the modeled pipe in this simulation, three-dimensional mode was used and the results were more accurate in this mode for modeling. The simulation was performed on a stainless steel pipe with a diameter of 500 mm and a length of 1,000 mm. Crack defects on the external and internal surfaces and corrosion defects and geometric anisotropy on the internal surface have been simulated in the mentioned pipes. Geometric anisotropy is given below. The smallest mesh size was used for this modeling to obtain more accurate results. The mesh size in this simulation was considered between  $\lambda/12$  and  $\lambda/20$ . In this simulation, the mesh size was first selected as  $\lambda/12$  and an acceptable answer was not obtained from the results. Then the mesh size  $\lambda/20$  was selected and an acceptable answer was obtained. The pipes are simulated to find the signal obtained from the defects. The defect in this simulation is modeled by using a new process and the definition of a circle with a thickness of 5 mm and a length of 20 mm, and the circular part in the settings for the material in the software is considered as air, in which the empty hole in the circle will be recognized as a defect. Fig. 9 shows an example of a 3 defect modeling for a pipe. Ultrasonic emission simulation requires piezoelectric transmitter modeling, in which the mechanism of piezoelectric operation is modeled by applying a transient excitation pulse to the surface of the structure. To model this pulse, it can be used the real

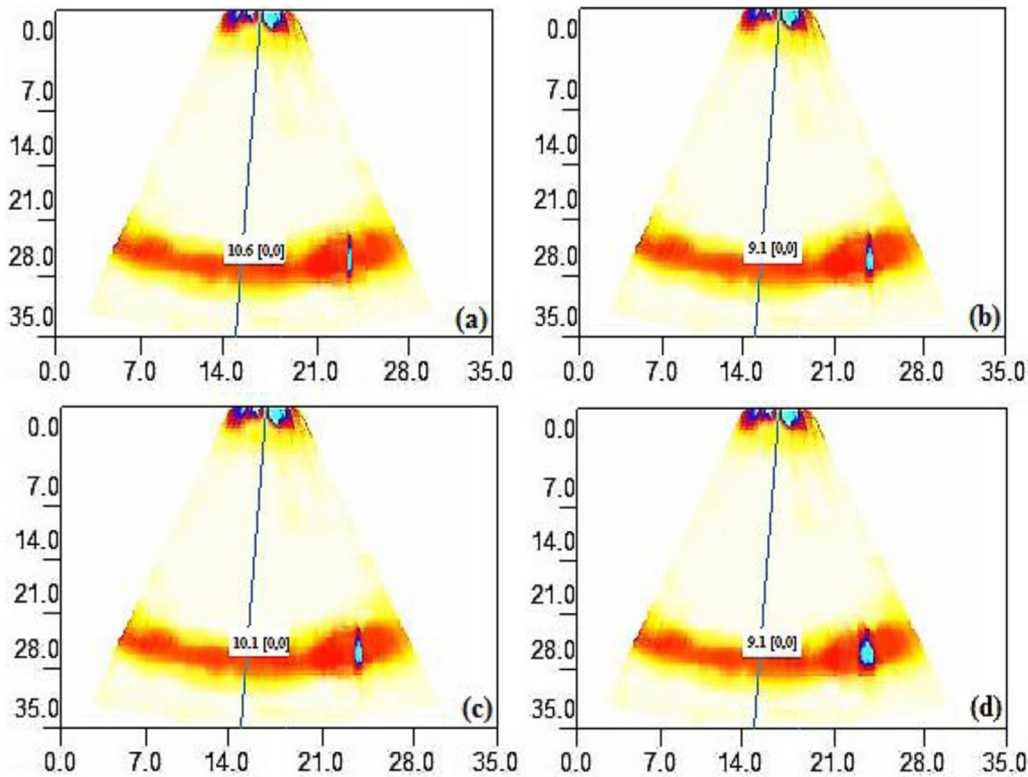


**Fig. 7.** Defect position and lack of knowledge of defect position: (a) results of Probe 1; (b) results of Probe 2; (c) results of Probe 3; and (d) results of Probe 4.

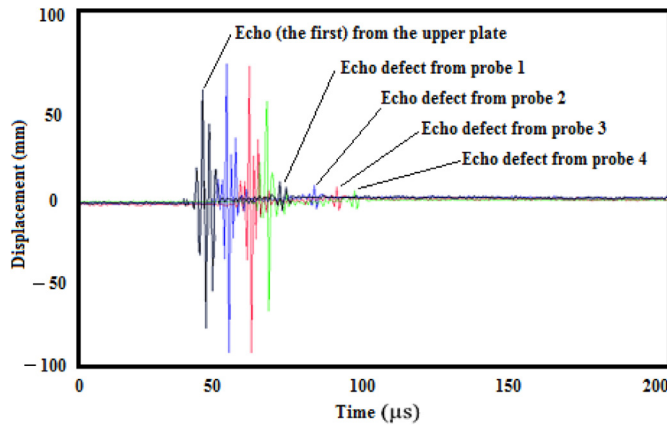


**Fig. 8.** Return echoes from corrosion defects.

transmitter pulse or an equation can be used for modeling. Using of a single-frequency function increases the concentration and consequently the wave energy, and ultimately allows for a longer pipe inspection. It should also be noted that if the excitation pulse has a lower bandwidth and its central frequency corresponds to the appropriate frequency, in addition to preventing the excitation of unwanted modes, it will also help reduce the effect of dispersion. To stimulate the probe, the Tone burst function is used, which leads to the focus and thus increases the energy of the wave. The desired function with sinusoidal period  $n = 5$ , center frequency  $f_c = 2$  MHz and delay time  $t = 0.139$  is described as Eq. (1) and the physical properties of the material for the stainless-steel pipe are given in Table 3 (Rao, 2004). The excitation pulse at a frequency of 2 MHz is shown in Fig. 10.

$$\left\{ \begin{array}{l} F(t) = 0.5 \sin(2\pi f_c t) \left[ 1 - \cos\left(\frac{2\pi t f_c}{n}\right) \right], \quad t \leq \frac{n}{f_c} \\ 0, \quad t > \frac{n}{f_c} \end{array} \right. \quad (1)$$

### 3.2. PAUT simulation method

The probe bars are placed together at the same distance  $w$ . If these rods are moved relative to each other at time intervals  $t$ , the path difference between adjacent beams is  $\delta t$ , where  $C$  can be obtained from the following equation:  $\theta$  is the propagation speed of the ultrasonic wave. Release angle calculated:

$$\sin \theta = \frac{C \delta t}{w} \quad (2)$$

Therefore, to direct the ultrasonic beam in a certain direction, the appropriate time delay can be obtained from this relationship (Myshkin et al., 2019). Smaller phase components have the greatest beam range. Therefore, they also have the highest angular energy, according to the speed of wave propagation, the delay time in the probe area with a width of 0.5 mm was considered to apply a displacement of 0.138 microseconds, and by defining the domains related to the nodes of the probe arrays in the mentioned area, loading was done at the end of the pipe. Four probes were used in the simulation and this is the first time that four simultaneous probes are used in the simulation to obtain the defects for the accuracy of the results. The acoustic forces are directed at each excitation point along the circumference of the pipe. Fig. 11 shows the exact placement of four probes on the pipe. In this method, the propagation of ultrasonic beam in the piece with a wedge angle of 30 degrees and by applying a time delay in the stimulation signal on the modeled probes was considered. The desired angle is considered to be 30 degrees, which is called ultrasonic beam orientation. Ultrasonic beam orientation is very common in the PAUT technique. The PAUT consists of several identical transducers that are adjacent to each other, which are excited in turn and separately but with phase differences relative to each other. By properly adjusting of this phase difference, the beams from these transmitters can be concentrated at the desired point, thus achieving images with separability and reliability. Stimulation of all points in each probe is applied in the form of 8, on each probe points are defined as  $8 \times 8$ , which will be the number of

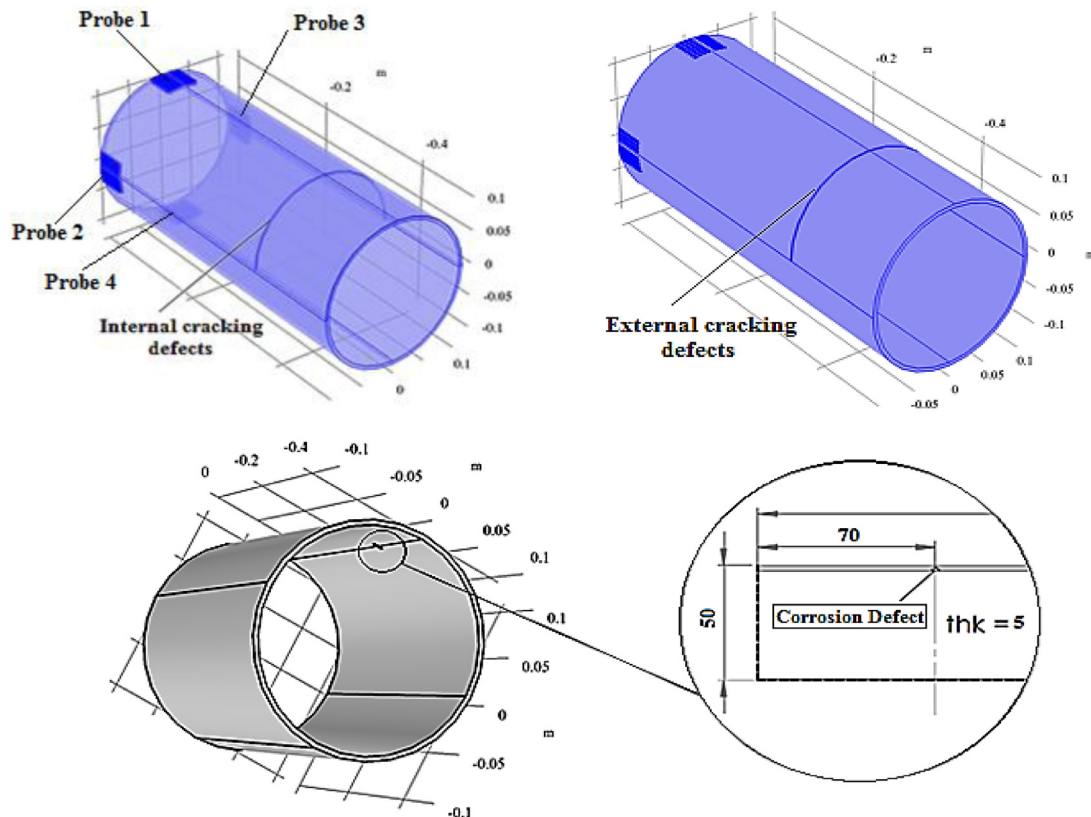


Fig. 9. Modeling of internal and external cracking defect and corrosion defect on the pipe.

**Table 3**  
Physical properties of materials for the stainless-steel pipe.

Density (kg/m <sup>3</sup> )	Poisson's ratio	Young's modulus (GPa)	Number of probes	Central frequency (MHz)	Number of piezoelectric
7,850	0.35	205	4	2	64

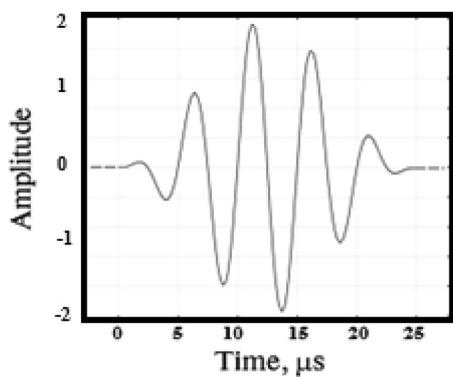


Fig. 10. Incitement pulse modeling (Gaussian pulse).

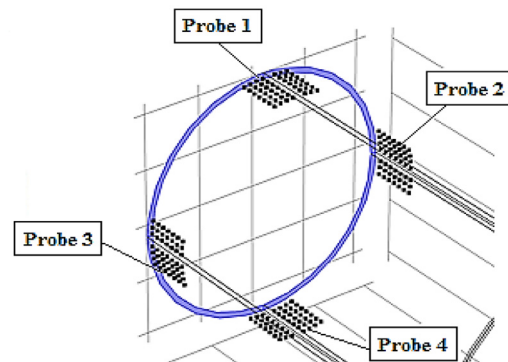
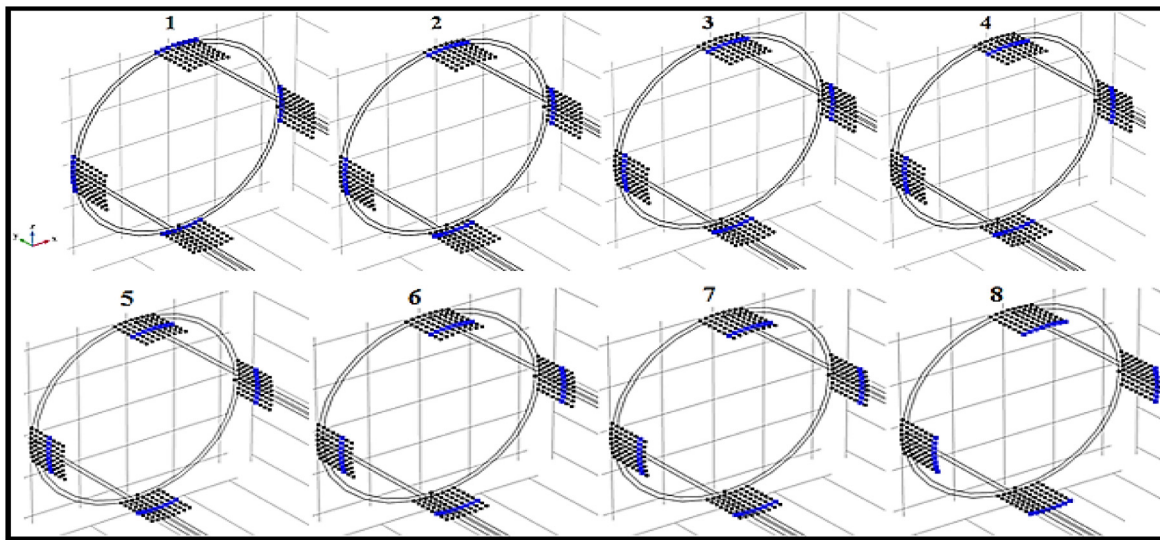


Fig. 11. Placement of four probes on the pipe.

elements. In this method, a probe with 64 elements with a delay time is considered according to Eq. (2), where 64 points are considered in the modeling. Each point has the authority of a probe and the numbers defined in Table 5 send the signal by considering Eq. (1). Other rows will send the wave with a time delay defined in the Comsol program, and signals and fault signals will be received. The steps for how to excite each point of the four probes and the definition of each of these points are shown in Fig. 12. Table 4 shows the selected number of individual probe points for activating and transmitting the wave. The

definition of each point, known as a probe, is required to send a wave with a time delay. By defining the total points and their delay time in the transmitted signals, the desired defect will be reached and the defect will be recognizable. Each probe has specific points and can send a wave by defining each point. When the delay time is applied to each of the points that we call probes, we must consider a number for each of them, so that the software considers one of these points randomly from each probe of 8 points or numbers and moves towards the defect according to the defined signal. In modeling, when the desired points are defined, random selection is done and considering that 256 points



**Fig. 12.** Defining the number of active points on four phased array ultrasonic probes.

**Table 4**

Selected number of each probe points to activate and send the wave.

Geometric entity level	Points
Probe 1–4 (no.1)	11, 26–27, 42–43, 58–59, 67, 79, 94–95, 110–111, 126–127, 150, 153, 168–169, 184–185, 200–201, 209, 221, 236–237, 252–253, 268–269, 280
Probe 1–4 (no.2)	10, 24–25, 40–41, 56–57, 66, 78, 92–93, 108–109, 124–125, 148–149, 166–167, 182–183, 198–199, 208, 220, 234–235, 250–251, 266–267, 279
Probe 1–4 (no.3)	9, 22–23, 38–39, 54–55, 65, 77, 90–91, 106–107, 122–123, 146–147, 164–165, 180–181, 196–197, 207, 219, 232–233, 248–249, 264–265, 278
Probe 1–4 (no.4)	8, 20–21, 36–37, 52–53, 64, 76, 88–89, 104–105, 120–121, 144–145, 162–163, 178–179, 194–195, 206, 218, 230–231, 246–247, 262–263, 277
Probe 1–4 (no.5)	7, 18–19, 34–35, 50–51, 63, 75, 86–87, 102–103, 118–119, 142–143, 160–161, 176–177, 192–193, 205, 217, 228–229, 244–245, 260–261, 276
Probe 1–4 (no.6)	6, 16–17, 32–33, 48–49, 62, 74, 84–85, 100–101, 116–117, 140–141, 158–159, 174–175, 190–191, 204, 216, 226–227, 242–243, 258–259, 275
Probe 1–4 (no.7)	5, 14–15, 30–31, 46–47, 61, 73, 82–83, 98–99, 114–115, 138–139, 156–157, 172–173, 188–189, 203, 215, 224–225, 240–241, 256–257, 274
Probe 1–4 (no.8)	4, 12–13, 28–29, 44–45, 60, 72, 80–81, 96–97, 112–113, 136–137, 154–155, 170–171, 186–187, 202, 214, 222–223, 238–239, 254–255, 273

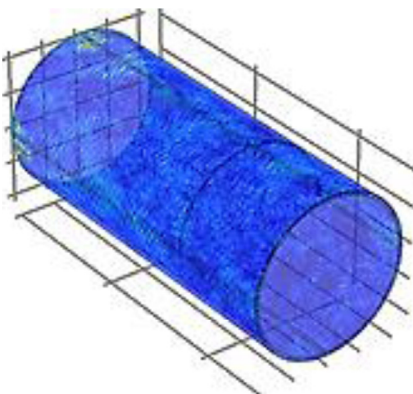


**Fig. 13.** Wave propagation in the pipe by four probes.

will be defined, random numbers are considered for each probe according to the delay time. For example, if the numbers 102–103 are placed together, it is certain that number 102 is from one probe and number 103 is from another probe. The propagation of waves in the pipe by four probes is shown in Fig. 13. The numbers in Table 2 show the exact size of the defect, if the size of the defect is different, their size will definitely change.

### 3.3. Receiving a defect signal from the simulation

Probe 1, 2, and 3 give us a complete and clear signal of the defect, but since the location of Probe 4 is farther away and a suitable place has not been determined for it, it does not reflect the wave of the defect well. It is possible for the wave to pass through the defect and not even

**Table 5**

Measurement of return echoes from simulation test.

Return echoes from internal and external crack defects (mm)	Return echoes from corrosion defects (mm)
36	20

be able to detect it, which has necessitated the presence of four probes to detect defects, internal and external cracking, and internal corrosion. Fig. 14 shows the signal of the three simulated defects. According to the return signals from the defect, this amount is smaller for the corrosion defect because it is very difficult to detect in the simulation and the wave return is associated with various definitions of the defect. The signals of the defect models are received by the waves sent in Eq. (1), which propagate in the pipe environment and hit the defect, and its signal is received. Each point where the probe is considered will send the signal according to the entered delay at the same time according to the points applied in Table 4 for four probes and the defect signal will be obtained. In the simulation of the measurement of return waves, internal and external cracks of 36 mm were reported. This measurement was obtained by sending 8 points, each point having a wave from one probe and 64 points from four probes with a time delay. For corrosion defects, this size was reported as 20 mm. These measurements are exactly along with the experimental results and they are in very good agreement. The measurement of returned echoes from the simulation test can be seen in Table 5.

### 4. Investigating the effect of SH-wave on geometric anisotropy in stainless steel

Investigation of SH-wave for stainless steels and the effect of anisotropy on its speed and speed deviation was simulated by COMSOL

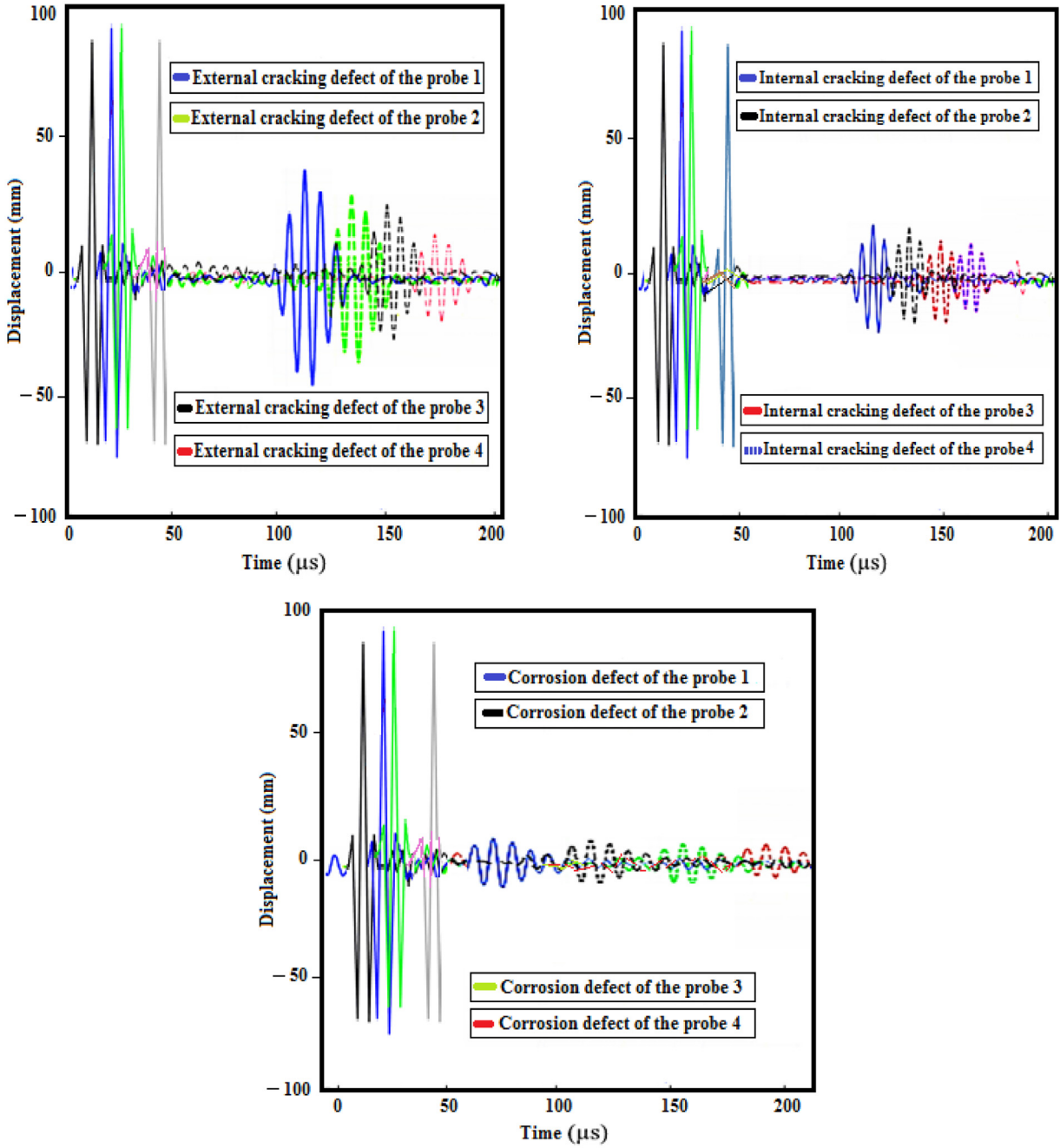
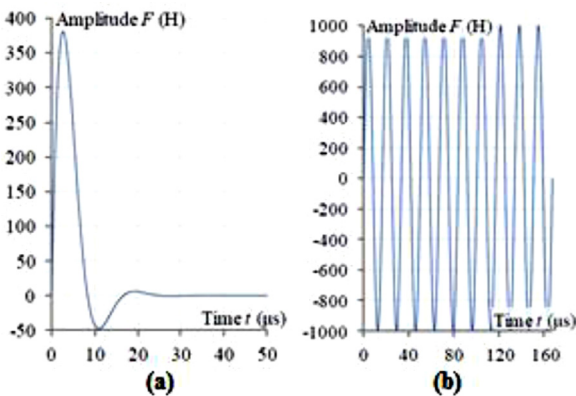


Fig. 14. The received signals are simulated from three defects.

software. A tangential force on the pipe surface at a fixed distance from its end surface was considered for the impact of these waves. The tangential force as a Berlage pulse with a frequency of 2 MHz to calculate the group velocity of SH-wave propagation is shown in Fig. 15. For the SH-wave radiation pattern, the phase velocity for a point source should be considered maximum in the direction of wave propagation, and it is zero in the direction perpendicular to it. In the simulation of the sound fields with the directions that are along the generatex and the tube surface, all angles were investigated. For the stainless steels used in this test, Young's modulus  $E = 205$  GPa, Poisson's ratio  $\eta = 0.31$  and density  $\rho = 8,070$  kg/m<sup>3</sup> were considered. The SH-wave speed in these tubes was 5,664 m/s and the wavelength at the main frequency was 56 mm. Paths and directions of wave propagation in pipe modeling between  $-90$  and  $90$  degrees and angle  $\alpha$  with 2 degrees step were determined in comparison with pipe genetics and their variability was considered according

to the desired degree. The velocities are obtained on the outer surface of the tube, and the interference of all waves with different modes can be used to check the SH-wave radiation pattern. Radiation patterns are obtained at a distance of 50 cm from the pipe to the source that we have defined for the propagation of these waves. Fig. 16 (a) shows the SH-wave radiation pattern along the pipe and Fig. 16 (b) shows the SH-wave radiation pattern along the pipe cover. The difference in the behavior of the radiation patterns of these two forms is due to the influence of the effect of geometric anisotropy on the amplitude of the signals. The radiation pattern of the wave for the pipe coating is simulated with the cosine function because its radiation pattern is similar to the radiation pattern of SH-waves. The opening width of the radiation pattern at the level of 5 dB is 40 degrees. Along the length of the tube, the radiation pattern practically does not depend on the angle up to 5 degrees, and the width of the radiation pattern opening at the 5 dB level is 36 de-



**Fig. 15.** Model of pulses (a) tangential forces pulse as a Berlage pulse (b) radio pulse.

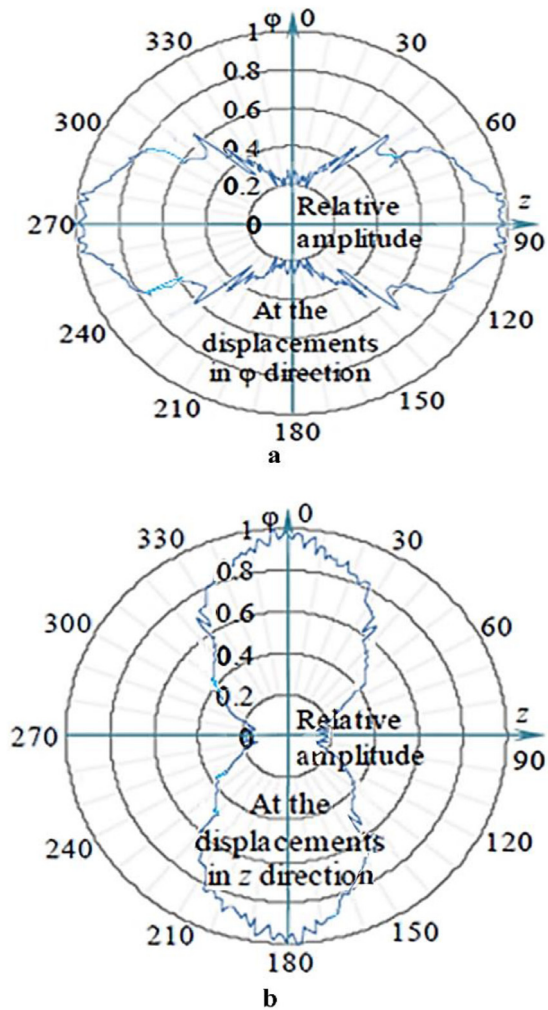


**Fig. 16.** Dependencies of the relative amplitude of the displacements at the radiation in the axial (a) and circumferential (b) directions from the angle of the wave propagation trajectory deviation from the pipe generatrix in the polar system.

grees. SH-wave recording angles and the critical angle is 76 degrees, which cannot be recorded above this angle. The smaller the diameter of the tube, the narrower the width of the radiation pattern, and the more linear the dependence of the amplitude on the angle. Fig. 17 shows the dependence of SH-wave propagation speed on the deviation angle of the wave propagation path from the tube generator. Increasing the devia-

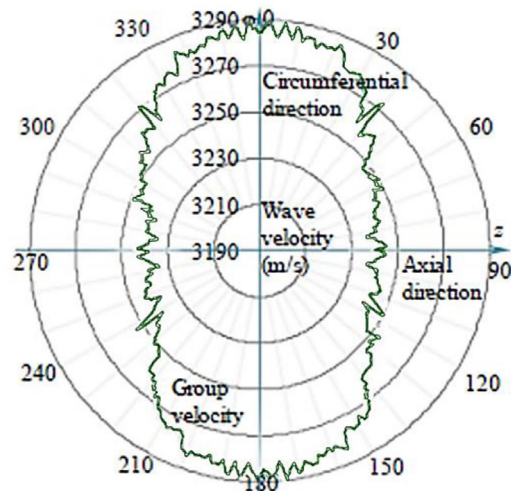


**Fig. 17.** Dependence of SH-wave speed in the polar system on deviation angle of wave propagation path from pipe generatrix.

tion angle in the simulation will lead to the growth of the angle to the non-linear direction and the speed of the group and phase will be observed as 46 and 58 m/s respectively. By increasing the distance along the thickness and wall of the pipe, we will face a drop in displacement. The reason for the drop in displacement, according to the investigations, is the reduction of the distance traveled by the wave compared to the external surface. The apparent velocity that was estimated at the beginning of the experiment increases with the increase of the angle. The smaller the tube radius and the higher the frequency, the greater the velocity deviation.

## 5. Conclusion

Experimental and simulation tests were carried out by four probes at different points of the pipe for internal corrosion defects and internal and external cracks. The simulation of the PAUT method by COMSOL software is a new method and in this article it was performed with a new solution and then the propagation behavior of ultrasonic waves was analyzed. Also, the results of geometric anisotropy for the tube were discussed and analyzed in this article. Detailed overall results of each test are given below:

- In this research, to improve the results and the reliability of the results, all the signals were sampled at a frequency of 2 MHz and four probes were used at four different points of the tube to obtain the defects.
- By placing and using four probes simultaneously on the pipe, the possibility of the wave passing through the defect is greatly reduced and it is easy to identify corrosion defects even if their size is small.
- According to the results of the experimental test, the best delay time and the time when the echo reaches the error is Probe 1. Also, Probe 4 does not reflect a good signal due to its distance from the defect detection location.
- From the experimental test results, it can be concluded that in order to identify the defect, the test must be performed several times to determine its exact amount. But this problem will be solved by using four probes.
- According to the simulation results, the corrosion defect was considered and modeled with a new simulation and an arc definition of the circle with the said depth, and by selecting the gender from the air, the considered area was known as the depth in the software so that the defect can be detected.
- To investigate longer lengths, the single-frequency function was used, which focused the wave and thus increased the energy of the wave.

- In the PAUT simulation method, according to the speed of wave propagation, the delay time in the transmitter area with a width of 0.5 mm was considered to apply a displacement of 2.5 microseconds, and by defining the respective ranges by the transfer arrays, loading was done on the pipe.
- To achieve the desired results, ultrasonic beam propagation in the tube was considered at an angle of 30 degrees. By properly adjusting the phase difference, the transmitter beams were focused at the desired point and images were created with high separation capability.
- In the probe modeling, 8 points are considered for each probe and  $8 \times 8$  points are defined on each probe, the number of which will be 64 elements. Each probe has specific points and the wave can be sent by defining each point.
- Experimental test results and numerical simulation show the correct implementation of PAUT for non-destructive analysis of pipes.
- The signals received from Probe 1, 2, and 3 are desirable and acceptable, but the signal received from Probe 4 does not reflect the wave well from the defect due to the probe's distance from the defect, and the transmitted wave may even pass through the defect and fail to detect the defect. For this reason, it is necessary to use four probes to test internal and external cracking as well as corrosion.
- In geometrical anisotropy, when the point source is stimulated, the SH-wave speed of the outer surface of the pipe is higher than the nominal speed of the inner surface of the pipe.
- The difference in SH-wave propagation speed on the inner and outer surface of the tube (along the generatrix and the tube cover) can be about 40 m/s. The greater the speed difference, the smaller the diameter and frequency of the tube and the thicker the wall.
- The speed increases with the increase of the angle and the deviation increases with the increase of the tube radius and the increase of the frequency.
- According to the results of the experimental test and simulation, a very good match between them is observed, and the ultrasonic phased array method can be used to determine the result of the non-destructive test.
- According to the measurement of return echo in internal and external cracks and corrosion defects, the error rate between the experimental test and simulation was reported to be 0.1 mm.

### Declaration of Competing Interest

The authors have no conflict of interest related to this manuscript.

### Ethical statement

Article was conducted according to ethical standards.

### Funding

There is no funding body for this submission.

### References

- Ahmed, O., Wang, X., Tran, M.V., Ismadi, M.Z., 2021. Advancements in fiber-reinforced polymer composite materials damage detection methods: towards achieving energy-efficient SHM systems. Composites Part B: Engineering 223, 109136.
- Azari, Hoda, Kok, Russell, 2022. "Implementation of American Association of State Highway and Transportation Officials/American Welding Society D1. 5 Phased Array Ultrasonic Weld Inspection Programs". Transportation Research Record, 03611981221090240.
- Brigante, M., Sumbatyan, M.A., 2013. Acoustic methods for the nondestructive testing of concrete: A review of foreign publications in the experimental field. Russian Journal of Nondestructive Testing 49 (2), 100–111.
- Chauveau, D., 2018. Review of NDT and process monitoring techniques usable to produce high-quality parts by welding or additive manufacturing. Welding in the World 62 (5), 1097–1118.
- Dolmatov, D.O., Tarrazó-Serrano, D., Filippov, G.A., Minin, I.V., Minin, O.V., Sednev, D.A., 2019. Application of Phase-Reversal Fresnel Zone Plates for Improving The Elevation Resolution in Ultrasonic Testing with Phased Arrays. Sensors 19 (23), 5080.
- Fendzi, C., Morel, J., Rébillat, M., Guskov, M., Mechbal, N., Coffignal, G., 2014. Optimal Sensors Placement to Enhance Damage Detection in Composite Plates, in 7th European Workshop on Structural Health Monitoring, pp. 1–8.
- Frederick, C., Porter, A., Zimmerman, D., 2010. High-density polyethylene piping butt-fusion joint examination using ultrasonic phased array. Journal of pressure vessel technology 132 (5).
- Groysman, A., 2019. Nondestructive Testing and Corrosion Monitoring. Non-Destructive Evaluation of Corrosion and Corrosion-assisted Cracking 261.
- Hakoda, C., Rose, J., Shokouhi, P., Lissenden, C., 2018. Using Floquet periodicity to easily calculate dispersion curves and wave structures of homogeneous waveguides. AIP Conference Proceedings 1, 020016.
- Liu, W., Wen, Z., Wang, J., Wang, S., Wang, H., Zhang, W., Hong, J., 2022. Experimental Study on Lateral Resolution of Phased Array Ultrasonic Testing of Irregular Structure Weld Defects. Shock and Vibration 2022.
- Liu, W., Wen, Z., Wang, J., Wang, S., Wang, H., Zhang, W., & Hong, J. (2022). Experimental Study on Lateral Resolution of Phased Array Ultrasonic Testing of Irregular Structure Weld Defects. Shock and Vibration, 2022.
- Malinowski, P., Wandowski, T., Trednafilova, I., Ostachowicz, W., 2009. A phased array-based method for damage detection and localization in thin plates. Structural Health Monitoring 8 (1), 5–15.
- Mirmahdi, E., 2020. Numerical and experimental modeling of spot welding defects by ultrasonic testing on similar sheets and dissimilar sheets. Russian Journal of Nondestructive Testing 56 (8), 620–634.
- Mirmahdi, E., 2021. Analysis and Examination of Aluminum Sheets Suitable for Automobile Body: Ultrasonic Testing, Signal Processing, Simulation. Russian Journal of Nondestructive Testing 57 (2), 135–144.
- Murav'eva, OV, Murav'ev, VV, 2016. Methodological peculiarities of using sh- and lamb waves when assessing the anisotropy of properties of flats. Russian Journal of Nondestructive Testing 7, 363–369.
- Myshkin, Y.V., Muravieva, O.V., Voronchikhin, S.Y., Samokrutov, A.A., Shevaldykin, V.G., 2019. Geometric anisotropy of velocity of horizontally polarized shear wave in pipe. Journal of Physics: Conference Series 1327 (1), 012023 VolNoIOP Publishing.
- Qin, Y., Shi, J., Zheng, J., Hou, D., Guo, W., 2019. An improved phased array ultrasonic testing technique for thick-wall polyethylene pipe used in nuclear power plant. Journal of Pressure Vessel Technology 141 (4).
- Rao, S.S., 2004. The finite element method in engineering. Elsevier Science & Technology Book's Fourth Edition.
- Rosa, B.M., Yang, G.Z., 2020. Towards integration of ultrasonic-powered implantable devices for physiological monitoring, stimulation, and imaging in soft tissues using a handheld scanning probe. IEEE Sensors Journal 21 (13), 14099–14109.
- Satyaranayran, L., Sridhar, C., Krishnamurthy, C.V., Balasubramaniam, K., 2007. Simulation of ultrasonic phased array technique for imaging and sizing of defects using longitudinal waves. International Journal of Pressure Vessels and Piping 84 (12), 716–729.
- Schabowicz, K., Suvorov, V.A., 2014. Nondestructive testing of a bottom surface and construction of its profile by ultrasonic tomography. Russian Journal of Nondestructive Testing 50 (2), 109–119.
- Shevtsov, S., Chebanenko, V., Shevtsova, M., Chang, S.H., Kirillova, E., Rozhkov, E., 2020. On the directivity of Lamb waves generated by wedge PZT actuator in thin CFRP panel. Materials 13 (4), 907.
- Shi, Y., Li, X., Zhang, J., 2020. Research on scanning path of automatic phased array ultrasonic testing of pipe welds with complex geometry. Russian Journal of Nondestructive Testing 56 (4), 340–349.
- Tran, M.Q., Agostinetti, P., Aiello, G., Avramidis, K., Baiocchi, B., Barbisan, M., Zhang, W., 2022. Status and future development of heating and current drive for the EU DEMO. Fusion Engineering and Design 180, 113159.
- Wilkinson, S., & Duke, S. M. (2014). Comparative testing of radiographic testing, ultrasonic testing and phased array advanced ultrasonic testing non destructive testing techniques in accordance with the AWS D1. 5 bridge welding code (No. BDK84-977-26). Florida. Dept. of Transportation.